A COMPARISON BETWEEN TRUE TRIAXIAL AND PLANE STRAIN COMPRESSION BY 3D DEM

Md. Mahmud SAZZAD[1] and Kiichi SUZUKI[2]
[1] Graduate Student, Department of Civil and Environmental Engineering, Saitama University
[2] Associate Professor, Department of Civil and Environmental Engineering, Saitama University

ABSTRACT

Granular materials such as sand experience different stress paths depending on the in-situ conditions. A granular system experiences true triaxial compression below a foundation whereas it experiences plane strain compression in dams or embankments of roads. This difference in the stress path affects the behavior of granular materials. The objective of this paper is to compare the behavior of granular materials under true triaxial and plane strain compression condition using 3D discrete element method (DEM). A cubical isotropically compressed dense sample consisting of 8000 spheres was prepared using periodic boundaries. True triaxial compression (TTC) and plane strain compression (PSC) tests were simulated using the same cubical sample to explore and compare the macro and micro responses of granular materials during shear with no bias from the initial fabric. The simulated macro results are consistent to that observed in the experimental studies. PSC test depicts higher peak stress ratio than TTC test. The b value at peak stress state for PSC is 0.396. The evolution of coordination number and sliding contact fraction is independent of stress paths. A linkage between macro and micro quantities is observed and a unique macro-micro relationship is noticed regardless of stress paths applied in this study.

KEYWORDS: TTC, PSC, Comparison, Micro response, DEM.

1. INTRODUCTION

Granular materials respond differently when they experience different stress paths. Below a foundation, the in-situ condition is representative of true triaxial compression test while in case of dams or embankments of roads; the in-situ condition corresponds well to the plane strain compression test. The difference in the mechanical responses due to the difference of stress paths has already been reported by several experimental studies. For example, Cornforth (1964) reported that internal friction angle is more than 4° greater for plane strain condition than triaxial condition in dense state. Peters et al. (1988) reported that shear band initiation is easier under plane strain condition than axis symmetric condition. Although several comparison based studies were performed in experimental works, they suffered from several shortcomings. For example, in experimental studies, the same sample can not be prepared for the TTC and PSC tests. However, it is very important to prepare same sample having the same initial fabric to avoid any discrepancy or biasness of the results in comparative based studies. This inherent limitation of experiments can be avoided using the numerical methods such as DEM (Cundall and Strack 1979), which has already been recognized as a useful tool in studying the behavior of granular materials. Besides, the evolution of micro variables can best be studied and compared using DEM. However, there are limited studies found in the literature that consider TTC and PSC using DEM. For example, Ng (2004) considered several stress paths with different sample preparation methods to investigate the macro and micro responses. This paper presents the comparison of macro and micro behavior of granular materials exclusively for TTC and PSC using 3D DEM. The macro responses including the dilatancy index, b value etc. are presented and the micro responses such as the coordination number, sliding contact fraction, contact fabric etc. are discussed. The linkage between the macro stress ratio and micro fabric ratio has also been presented.

2. BRIEF IDEA ABOUT DEM

In the present study, DEM is used to model the behavior of granular materials. DEM is a numerical technique pioneered by Cundall and Strack (1979), which has been used in different disciples of science and engineering. The major advantage of DEM is that the kinematics of each

particle can be monitored and extracted at any step during the simulation. DEM based studies have been widely used to enhance our understanding and explain the experimentally observed phenomena from micro point of view. The detailed explanation of DEM was described in Cundall and Strack (1979). The basic idea of DEM is very simple. In DEM, each particle is modeled as an element. An element in DEM can make and break contact with other elements involved in the model. The calculation cycle in DEM involves the alternate use of Newton's second law of motion and a force displacement law. The translational and rotational accelerations of particles are computed using the following expressions:

$$m\ddot{x}_i = \sum F_i \quad i = 1,3 \tag{1}$$

$$I\ddot{\theta} = \sum M \tag{2}$$

where, F_i are the force components on each particle; M is the moment on each particle; m is the mass; I is the moment of inertia; $\ddot{x}_i$ are the components of translational acceleration and $\ddot{\theta}$ is the rotational acceleration of the particle.

3. ABOUT COMPUTER PROGRAM

In this study, computer program OVAL (Kuhn 2006) is used which can perform DEM analysis of particle assemblies. The program is written in FORTRAN and can run both in windows and Linux platform. The effectiveness of OVAL has already been recognized (e.g., Kuhn 1999; Kuhn 2005). A simple contact model consisting of two linear springs, one in normal direction and other in tangential direction and a frictional slider has been incorporated. The deformation can be applied either using a deformation rate tensor or using a stress rate tensor. The viscosity coefficient for translational and rotational body damping used in the program represents a fraction of the critical damping $2\sqrt{mk_n}$ and $2r\sqrt{Ik_t}$ where r, k_n and k_t denote the radius, normal and tangential contact stiffness of the particle, respectively.

4. SAMPLE PREPARATION METHOD

A cubical sample consisting of 8000 spheres of 16 different sizes (diameters) ranging from 3 to 4.5 mm was prepared. At first, the spheres were placed at the equally spaced grid points of a cubical frame. The sizes of spheres were chosen randomly. The initial sample generated in this way was very sparse. The initial sparse sample was compressed isotropically to 100 kPa using periodic boundaries in different stages. The interparticle friction was intentionally turned off during the preparation of the isotropically compressed sample so that the particles were packed in a dense state and the sample could be regarded as dense. Desired interparticle friction coefficient was used later during shear. The void ratio and coordination number of the isotropically compressed dense sample are 0.57 and 5.94, respectively.

5. NUMERICAL SIMULATIONS

Same isotropically compressed dense sample was used for the simulation of TTC and PSC tests so that the initial fabric of the sample prior to shear remains identical. Simulation of TTC test was carried out by reducing the sample height slowly downward with a small strain increment of 0.00002% in vertical direction (x_1-direction) while keeping the lateral stress in x_2- and x_3-direction constant (100 kPa). On the other hand, simulation of PSC test was carried out by reducing the sample height with the same strain increment downward vertically while maintaining the stress in x_3-direction constant (100 kPa) and keeping the strain in x_2-direction zero (i.e. $d\varepsilon_2$=0). The simulation condition of TTC and PSC tests with reference axes is depicted in Figure 1 as well for clarity. The DEM parameters used in the numerical study are shown in Table 1.

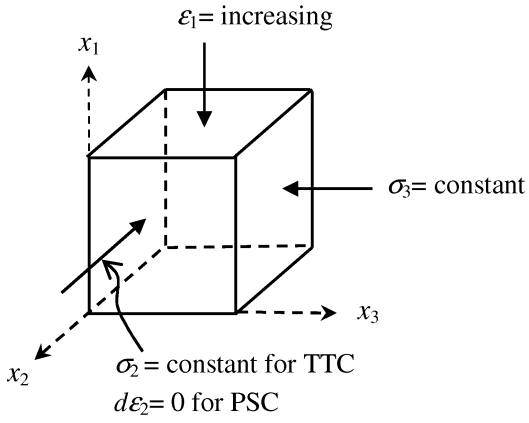

Figure 1 A cubical element with simulation conditions and reference axes.

Table 1 DEM parameters used in the study

DEM parameters	Value
Normal contact stiffness (N/m)	1×10^6
Tangential contact stiffness (N/m)	1×10^6
Mass density (kg/m^3)	2650
Increment of time step (s)	1×10^{-6}
Interparticle friction coefficient	0.50
Coefficient of viscosity for translational and rotational body damping	0.05

6. MACRO RESPONSES

6.1 Stress-strain-dilative behavior

The simulated stress-strain behavior for true triaxial and plane strain condition is depicted in Figure 2. For both the cases, the stress ratio σ_1/σ_3 increases with axial strain ε_1 followed by strain softening, where σ_1 and σ_3 are the stresses in x_1- and x_3-direction, respectively. However, softening behavior is dominant and clear in case of PSC test. This tendency is consistent with the experimental observation (e.g., Cornforth 1964). It is also noted that the plane strain condition gives higher stress ratio at peak state than true triaxial condition during the simulation. The change of strain in x_2-direction is maintained zero throughout the simulation of PSC test which allows to form a stable column-like structure compared to TTC test during shear and this may the probable reason why the stress ratio in case of PSC test is higher than TTC test.

The strains in x_1, x_2 and x_3 directions are represented by ε_1, ε_2 and ε_3, respectively and evolution of these strains for TTC and PSC tests is shown in Figure 3. Only 5% of ε_1 is considered in the plot for the clear view. It is noted in Figure 3 that the change of ε_2 for PSC test remains zero throughout the test as required. The evolution of ε_3 is same as ε_2 for TTC test as expected. It demonstrates the ability of DEM to simulate qualitatively the experimental observations for the dense sample.

The evolution of volumetric strain ε_v with ε_1 for TTC and PSC tests is depicted in Figure 4. Here, $\varepsilon_v = dv/v$, where v is the initial volume of the dense sample prior to shear and dv is the change of volume during the shear. A positive value ε_v in Figure 4 represents compression while a negative value of ε_v represents dilation. It is noted that dilation in case of PSC test overrides the dilation in case of TTC test, although the difference is small.

The evolution of dilatancy index ($DI = -d\varepsilon_v/d\varepsilon_1$) with ε_1 is depicted in Figure 5, where $d\varepsilon_v$ is the change of volumetric strain and $d\varepsilon_1$ is the change of axial strain. It is noted that the tendency of the evolution of dilatancy index is independent of the stress paths applied in this study.

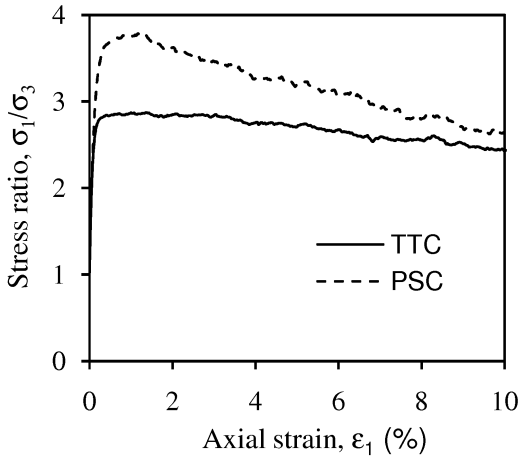

Figure 2 Stress-strain behavior for TTC and PSC tests

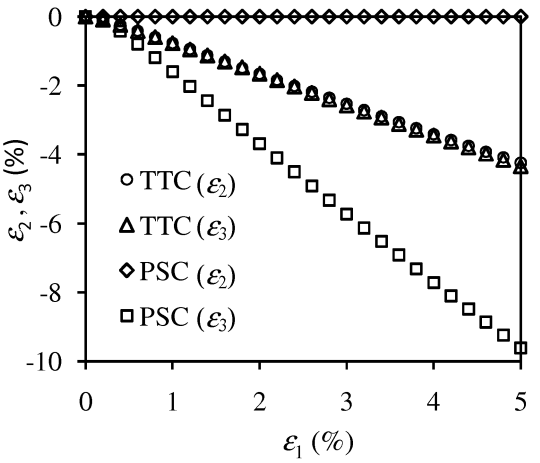

Figure 3 Evolution of strains for TTC and PSC tests

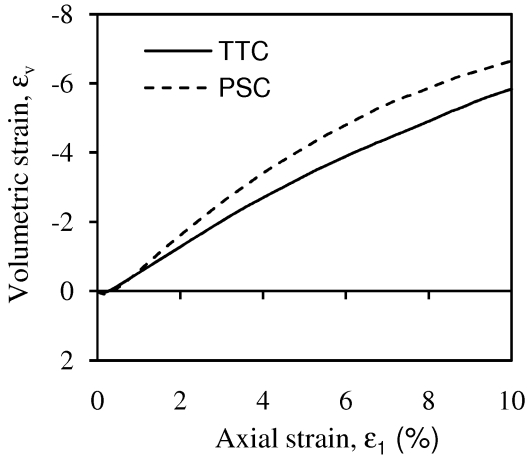

Figure 4 Evolution of volumetric strain for TTC and PSC tests

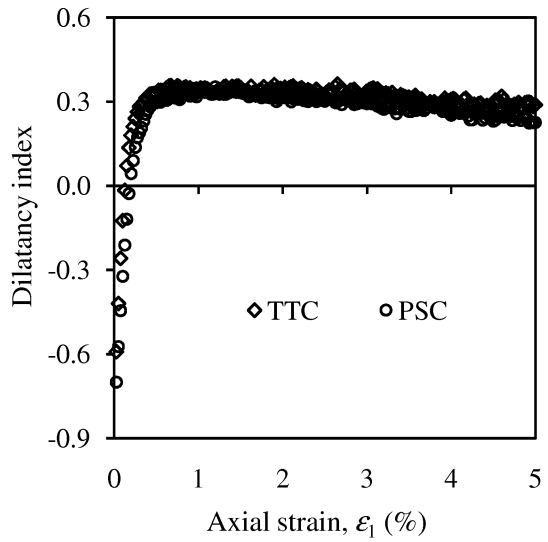

Figure 5 Evolution of dilatancy index for TTC and PSC tests

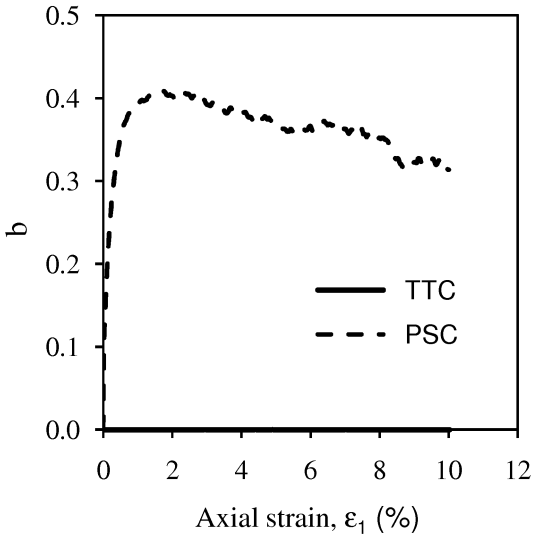

Figure 6 Evolution of b value with ε_1 for TTC and PSC tests

6.2 Evolution of *b* value

The term 'b' was first introduced by Habib (1953) and defined in the non-dimensional form as follows:

$$b = \frac{\sigma_2 - \sigma_3}{\sigma_1 - \sigma_3} \tag{3}$$

In TTC test, $\sigma_2 = \sigma_3$. Consequently, b value should be zero throughout the test. However, in PSC test, b value is not constant, rather variable. In the present numerical study, the evolution of b value with ε_1 is computed and depicted in Figure 6. It is noted that b value remains constant throughout the numerical simulation for TTC test as expected. However, b value varies with ε_1 for PSC test and the evolution tendency of b value with ε_1 has nice similarity, at least in a qualitative sense, to that of σ_1/σ_3 with ε_1. The b value gradually increases with the increase of ε_1 until it reaches a peak value and beyond the peak, b value reduces with the increase of ε_1. The b value at the peak stress state is 0.396 while the same at 10% axial strain is 0.314 for PSC test.

7. MICRO RESPONSES

7.1 Evolution of coordination number

The evolution of coordination number with ε_1 for TTC and PSC tests is depicted in Figure 7. Coordination number is defined as twice the total number of contacts to the total number of particles used in the simulation.

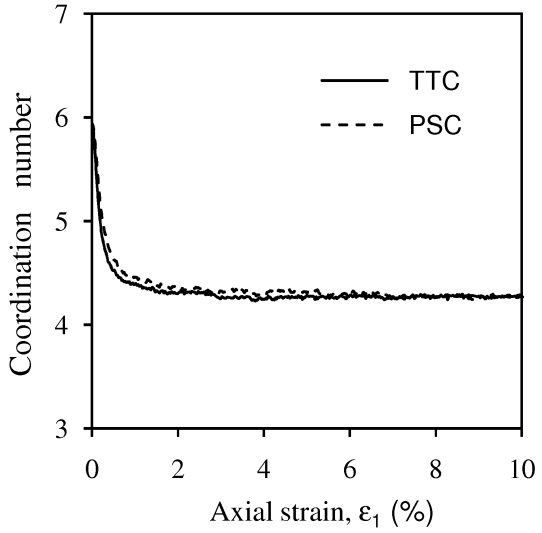

Figure 7 Evolution of coordination number with ε_1 for TTC and PSC tests

It is noted that coordination number decreases significantly at the beginning stage of simulation regardless of stress paths applied during the simulation which may be due to the rearrangement of fabric. Later, the change of coordination number becomes almost steady. It should also be noted that the evolution of coordination number is independent of stress paths applied (i.e., TTC and PSC) during the simulation.

7.2 Evolution of sliding contact fraction

The evolution of sliding contact fraction for TTC and PSC tests is depicted in Figure 8. Sliding contact fraction is defined here as the number of sliding contacts to the number of contacts at a given state of simulation. The sliding contact

fraction in the plot is expressed in percentage. It is noted that the evolution of sliding contact fraction is independent of whether the simulation is conducted in TTC condition or PSC condition.

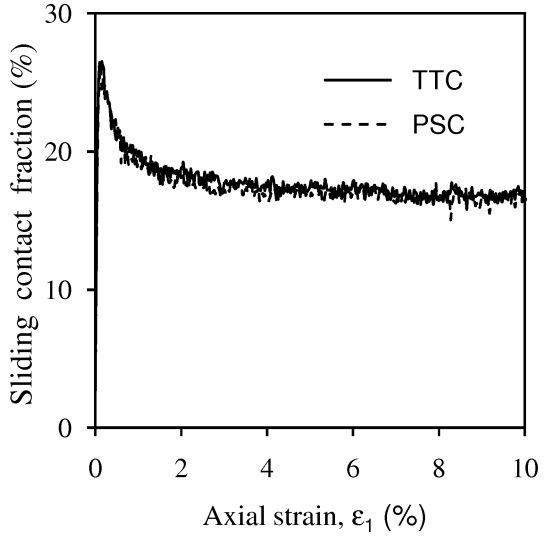

Figure 8 Evolution of sliding contact fraction with ε_1 for TTC and PSC tests

7.3 Evolution of contact fabric

The evolution of contact fabric for TTC and PSC tests is described in this section. The evolution of contact fabric is usually quantified using the fabric tensor given by Satake (1982) considering all contacts as follows:

$$H_{ij} = \frac{1}{N_c}\sum_{\alpha=1}^{N_c} n_i^{\alpha} n_j^{\alpha} \tag{4}$$

where n_i^{α} is the components of unit normal vector at $\alpha-$th contact and N_c is the number of contacts.

The contacts in a granular system can be further characterized as the strong contacts and the weak contacts to quantify their individual role (e.g., Radjai et al. 1998, Antony 2000, Antony et al. 2004, Azema et al. 2007). In the present study, a contact is defined as a strong contact if the normal contact force for a given contact is greater than the average normal contact force while a contact is defined as a weak contact if the normal contact force for a given contact is less than or equal to the average normal contact force. The average normal contact force is calculated as follows:

$$f_{ave}^{n} = \frac{1}{N_c}\sum_{i=1}^{N_c} f_i^{n} \tag{5}$$

where f_i^n is the normal contact force at i-th contact and f_{ave}^n is the average normal contact force considering all contacts.

Based on the classification of the total contacts into strong and weak contacts, two additional fabric tensors for the strong and weak contacts can be defined. The fabric tensor for strong contacts can be defined as follows (Kuhn 2006):

$$H_{ij}^{s} = \frac{1}{N_c}\sum_{s=1}^{N_c^s} n_i^s n_j^s \tag{6}$$

where, n_i^s is the components of unit normal vector at s-th strong contact and N_c^s is the number of strong contacts. Similar to the fabric tensor for strong contacts, the fabric tensor for the weak contacts can also be defined as follows:

$$H_{ij}^{w} = \frac{1}{N_c}\sum_{w=1}^{N_c^w} n_i^w n_j^w \tag{7}$$

where, n_i^w is the components of unit normal vector at w-th weak contact and N_c^w is the number of weak contacts.

Figure 9 depicts the evolution of fabric ratio H_{11}/H_{33} with ε_1 for TTC and PSC tests considering all contacts. It is noted that the fabric ratio H_{11}/H_{33} is almost 1.0 at zero strain level, which indicates the isotropic distribution of contact fabric prior to shear. A value grater than 1.0 or less than 1.0 indicates the anisotropic distribution of contact fabric.

In Figure 9, it is noted that H_{11}/H_{33} gradually increases with ε_1 until it reaches the peak value and then decreases with ε_1 regardless of the TTC or PSC conditions. This increase of H_{11}/H_{33} with ε_1 is the consequence of the formation of new contacts in vertical direction (x_1 -direction) and disintegration of contacts in lateral direction. However, the dominant evolution of H_{11}/H_{33} is noticed for PSC condition. A comparison of Figure 9 with Figure 2 depicts that the shape of the curves of these two figures are not matching well with each other. For example, the stress ratio peaks at the small strain level as seen in Figure 2 whereas the fabric ratio peaks at a large strain when all contacts are considered as seen in Figure 9.

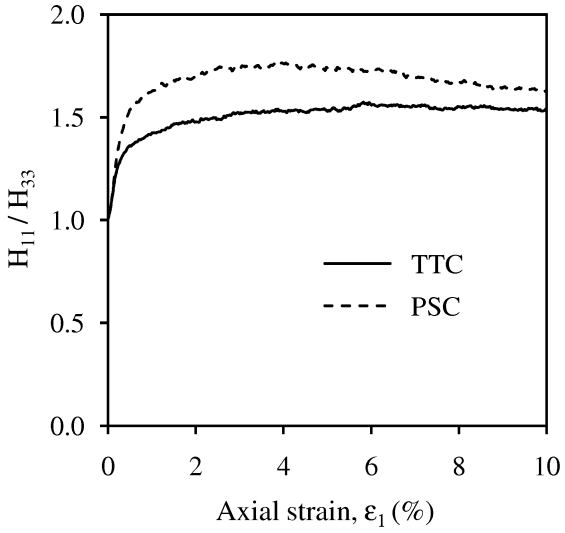

Figure9 Evolution of fabric ratio H_{11}/H_{33} with ε_1 for TTC and PSC tests

Figure 10, on the other hand, depicts the evolution of fabric ratio H_{11}^s/H_{33}^s with ε_1 for TTC and PSC tests considering only the strong contacts. A comparison of Figure 10 with Figure 2 shows a strong correlation between the stress ratio-axial strain curve and the fabric ratio-axial strain curve for strong contacts regardless of stress paths applied during the simulation. It is also noted that the anisotropy induced during PSC test is larger than that during TTC test. This large difference in the evolution of induced anisotropy in PSC test may be the consequence of the restriction of boundary movement in x_2-direction. The higher peak stress in case of PSC test may be the consequence of such dominant evolution of induced anisotropy in case of PSC test.

Figure 11 depicts the evolution of fabric ratio H_{11}^w/H_{33}^w with ε_1 for TTC and PSC tests considering the weak contacts only. It is noted that the fabric ratio is even smaller than 1.0 at the initial stage of simulation. This indicates that the anisotropy induced considering weak contacts at the initial stage of simulation has an opposite privilege direction compared to the privilege direction of the induced anisotropy considering strong contacts. However, it is noted in Figure 11 that the fabric ratio H_{11}^w/H_{33}^w gradually increases with ε_1 and becomes more than 1.0 as strain increases. It indicates that the privilege direction of induced fabric anisotropy for weak contacts gradually changes its direction as strain increases. Dominant induced fabric anisotropy is also developed for weak contacts in case of PSC test; however, the difference is very small as compared to the difference noticed in case of strong contacts.

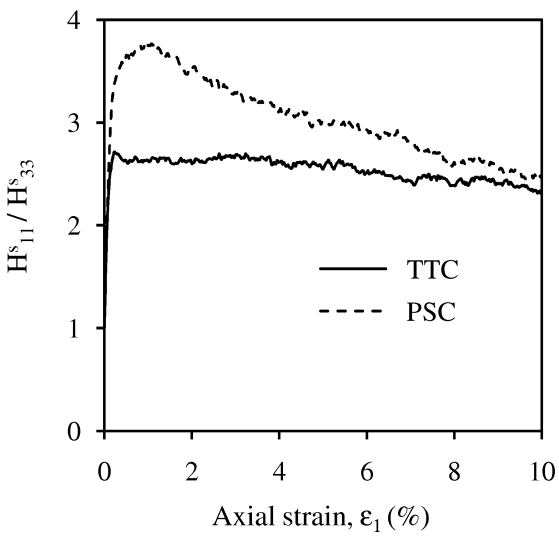

Figure 10 Evolution of fabric ratio H_{11}^s/H_{33}^s with ε_1 for TTC and PSC tests

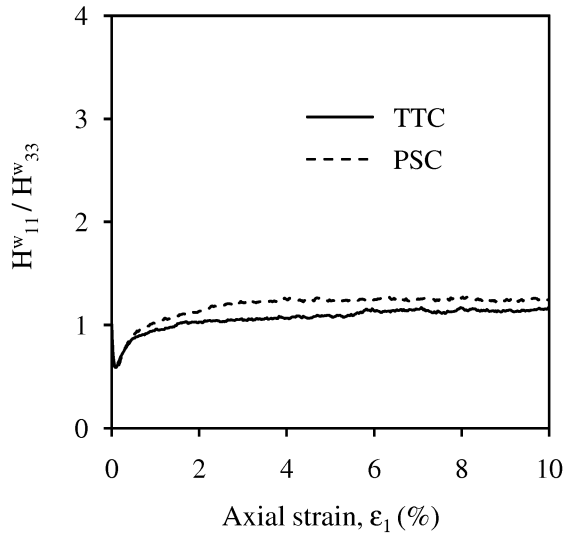

Figure 11 Evolution of fabric ratio H_{11}^w/H_{33}^w with ε_1 for TTC and PSC tests

8. MACRO-MICRO RELATIONSHIP

Since a strong correlation is noticed between the stress ratio-axial strain curve and fabric ratio-axial strain curve for strong contacts in Figure 10, it is intended to establish a macro-micro relationship for TTC and PSC tests considering strong contacts. Figure 12 depicts the relationship between the stress ratio σ_1/σ_3 and fabric ratio H_{11}^s/H_{33}^s considering strong contacts. For clear view, data upto 1% of axial strain is depicted in Figure 12. A unique macro-micro relationship is noticed regardless of the stress paths applied in the present study.

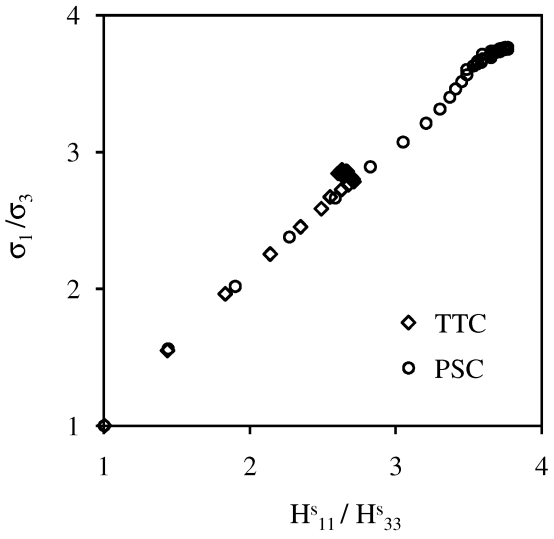

Figure 12 Relationship between the stress ratio σ_1/σ_3 and fabric ratio H_{11}^s/H_{33}^s considering strong contacts for TTC and PSC tests

9. CONCLUSIONS

Simulations of TTC and PSC tests are conducted in the present study to compare the macro and micro mechanical responses of granular materials for dense sample without a bias from the initial fabric of the sample prior to shear. The simulated macro results are consistent to that observed in the experimental studies in a qualitative sense, which demonstrates the versatility of simulated results of the present study. Some of the points of this study can be summarized as follows:

i) The tendency of the evolution of dilatancy index is independent of stress paths applied in the present study (i.e., TTC and PSC).

ii) The evolution of b value with ε_1 has nice similarity to that of σ_1/σ_3 with ε_1 for PSC test.

iii) The evolution of coordination number and sliding contact fraction is independent of the stress paths applied during the simulation.

iv) The fabric ratio evolves during PSC test is larger than that during TTC test considering all, strong and weak contacts.

v) The shape of fabric ratio-axial strain curve has sticking similarity to that of the stress ratio-axial strain curve when strong contacts are considered.

vi) A unique macro-micro relationship between stress ratio and fabric ratio exists regardless of the stress paths applied in the present study.

10. REFERENCES

Antony, S. J., (2000) "Evolution of force distribution in three-dimension granular media," *Physical Review E*, **V.** 63, (No. 1), 011302:1-13.

Antony, S. J., Momoh, R. O. and Kuhn, M. R., (2004) "Micromechanical modelling of oval particulates subjected to bi-axial compression," *Computational Materials Science*, **V.** 29, (No. 4), pp. 494-498.

Azema, E., Radjai, F., Peyroux, R. and Saussine, G, (2007) "Force transmission in a packing of pentagonal particles," *Physical Review* E, **V.** 76, (No. 1), 011301:1-13.

Cornforth, D. H., (1964) "Some experiments on the influence of strain conditions on the strength of sand," *Geotechnique*, **V.** 14**,** (No. 2), pp. 143–167.

Cundall, P. A. and Strack, O. D. L., (1979) "A discrete numerical model for granular assemblies," *Geotechnique*, **V.** 29, (No. 1), pp. 47-65.

Habib, P., (1953) "Influence of the variation of the average principal stress upon the shearing strength of soils," [in French] *Proceedings of the 3rd International Conference on Soil Mechanics and Foundation Engineering*, **V.** 1, pp. 131-136.

Kuhn, M. R, (1999) "Structured deformation in granular materials," *Mechanics of Materials*, **V.** 31, (No. 6), pp. 407-429.

Kuhn, M. R., (2005) "Are granular materials simple? An experimental study of strain gradient effects and localization," *Mechanics of Materials*, **V.** 37, (No. 5), pp. 607-627.

Kuhn, M. R., (2006) "OVAL and OVALPLOT: Programs for analyzing dense particle assemblies with the discrete element method."
http://faculty.up.edu/kuhn/oval/doc/oval_0618.pdf .

Ng, T. -T., (2004) "Macro- and micro-behaviors of granular materials under different sample preparation methods and stress paths," *International Journal of Solids and Structures*, **V.** 41, (No. 21), pp. 5871-5884.

Peters, J. F., Lade, P. V. and Bro, A., (1988) "Shear Band Formation in Triaxial and Plane Strain Tests," *Advanced Triaxial Testing of Soil and Rock*, ASTM STP977, Robert T., Donaghe, Ronald C., Chancy and Marshall L. Silver Eds., Philadelphia, pp. 604-627.

Radjai, F., Wolf, D. E., Jean, M. and Moreau, J. J, (1998) "Bimodal character of stress transmission in granular packings," *Physical Review Letters*, **V.** 80, (No. 1), pp. 61-64.

Satake, M., (1982) "Fabric tensor in granular materials," *Proceeding of IUTAM Symposium on Deformation and Failure of Granular Materials*, Delft, Balkema, pp. 63–68.